AIAA-99-4227

RAPID ENERGY DISSIPATION IN A YO-YO-TYPE WIRE BOOM DEPLOYMENT SYSTEM

by Mark L. Psiaki*, Paul M. Kintner, Jr.#, and Steven P. Powell**

Cornell University, Ithaca, N.Y. 14853-7501

Abstract

A wire boom deployment system has been developed that uses a mechanism which is similar to the classic yo-yo despin mechanism. The goal has been to develop a way to rapidly deploy wire booms from a spinning sounding-rocket experiment. The main challenge in using a yo-yo-type mechanism is to dissipate the excess kinetic energy so that the wire booms do not re-wrap themselves about the spacecraft after deploying. A ring has been added to the basic yo-yo mechanism. It rotates with respect to the main spacecraft about the nominal spin axis, and the wire booms deploy from it. The ring/spacecraft joint is damped, and relative motion between the ring and the spacecraft dissipates the excess energy. This system is analyzed and simulated in 2 and 3 dimensions. Techniques are developed for tuning the damping law to rapidly deploy the wire booms without the occurrence of re-wrapping, and a criterion is presented that ensures 3-dimensional stability of the final equilibrium in the global minimum-energy sense. Simulation results show that the system can deploy *2.5 m* wire booms in under 20 sec and that the deployment can tolerate the expected levels of asymmetry in the system configuration and the initial state.

Introduction

Most spacecraft need to deploy devices after launch in order to overcome the size constraints that are imposed by a booster's fairing. Wire booms are one type of deployable structure. Wire booms are long wires whose bases are attached to a spin-stabilized spacecraft. Normally a wire boom also has a tip mass at its end. Centrifugal force acts to keep the wire booms taut, Fig. 1. Wire booms are attractive because they can be built using very little mass per unit length. They have been used on a number of spacecraft missions, e.g., see Refs. 1 and 2.

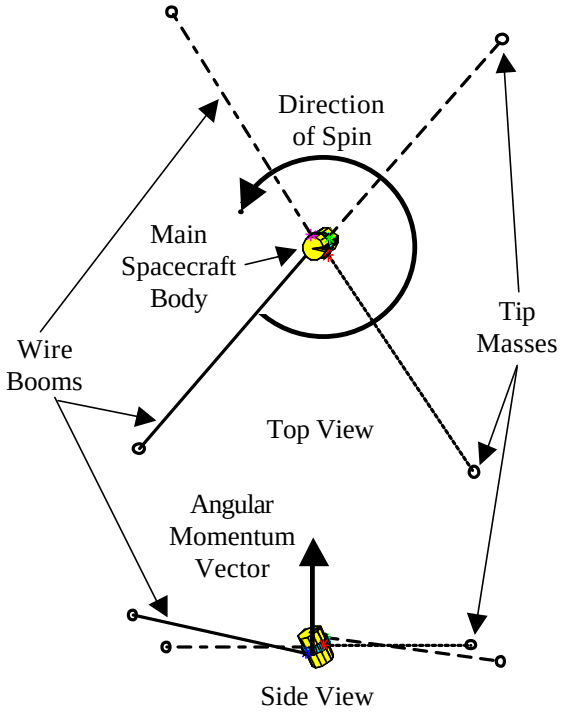

Fig. 1. Two views of a spacecraft with 4 wire booms and a yo-yo-type deployment mechanism. (shown during an asymmetric deployment at the time of maximum out-of-plane pendulum angle)

The current study of wire boom deployment is motivated by a desire to use wire booms on small "daughter" spacecraft in a sounding-rocket study of the ionosphere. This study is called "Sounding of the Ion Energization Region: Resolving Ambiguities" (SIERRA). The sounding rocket will deploy several small spin-stabilized free-flying daughter modules. Each of these will deploy 4 wire booms with electric probes at the end of each boom. The electric probes will be used to measure the electric field. The use of several daughter spacecraft will allow the system to resolve spatial/temporal ambiguities in observed variations of the electric field.

Current sounding rocket technology uses telescoping booms and other types of rigid booms. These booms are too heavy for use on small daughter modules, which is why wire booms are planned for use on this experiment.

---

* Associate Professor, Sibley School of Mechanical and Aerospace Engineering. Associate Fellow, AIAA.

Professor, School of Electrical Engineering.

** Research Support Specialist, School of Electrical Engineering.

The use of wire booms on a sounding rocket presents a major technical challenge in terms of deployment time. The IMP-J spacecraft mission planned to use an hour in order to deploy its 4 wire booms [1], and the Dynamics Explorer A spacecraft mission planned to deploy its 2 wire booms in stages during a two-week period [2]. By contrast, a typical sounding rocket flight lasts a total of about 1,000 sec. Therefore, the wire booms would need to deploy in a fraction of that time, in 100 sec or less.

The yo-yo despin system presents an attractive model for a possible wire boom deployment system. Yo-yo systems are commonly used for lowering the spin rate of a spinning spacecraft [3-6]. These systems consist of 2 or more wires whose bases are initially attached to the spacecraft and whose ends have a tip mass. Initially they are wrapped around the circumference of the spinning spacecraft in a direction opposite to that of the spacecraft spin vector. The tip masses are held in place initially. When their restraints are severed, the yo-yos start to unwrap and the spacecraft's spin rate decreases. When the cables are fully unwrapped, their bases are released, and they fly away from the spacecraft. The final spacecraft angular velocity is greatly reduced, and all of this happens in a matter of a few seconds.

It is necessary to add an energy dissipation mechanism to the yo-yo system in order to use it for wire boom deployment. In the despin system the yo-yos carry away any excess energy when they are released from the spacecraft. Without energy dissipation, retained yo-yos would have excess energy when they reached their fully deployed state, and they would re-wrap around the spacecraft in the opposite direction from their initial wrapping. During this re-wrapping the wire booms might become entangled, which would cause a deployment failure.

Energy dissipation can be added to the yo-yo deployment mechanism by using a ring with a rotary damper. The idea is to wrap the wires around a ring that is free to rotate with respect to the main spacecraft about the spin axis, Fig. 2. This rotation is restrained only by a damper. The main spacecraft body begins with a counter-clockwise angular velocity. The ring starts out with the same angular velocity, but when the yo-yo tip masses get released and start to unwrap, the tension in their cables causes the ring's direction of rotation to reverse and become clockwise. This causes relative motion between the ring and the main spacecraft body, as depicted by the figure's arrows. The relative rotation causes energy dissipation in the rotary damper. If the damping is tuned correctly, then the excess energy will be almost totally dissipated when the yo-yos first reach their deployed position, and they will not re-wrap about the spacecraft.

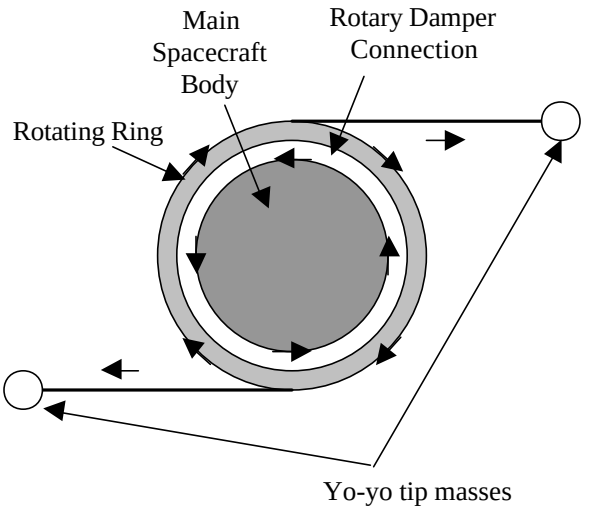

Fig. 2. Yo-yo wire boom deployment mechanism with damped ring for energy dissipation.

The contributions of this paper are to develop a mathematical model for this wire boom deployment system and to analyze and simulate it. Several important issues are investigated. One of them is to determine whether deployment can be achieved without re-wrapping of the cables and to determine the achievable deployment times. This analysis will show how to tune the system to get good performance, and it will consider the sensitivity of the performance to parameter uncertainty.

The rest of the issues that will be considered have to do with three-dimensional motions of the system. One important issue is the final 3-D stability of the resulting configuration. If designed improperly, then the system can end up in a canted or flat spin with its wire booms in the wrong locations, or its lightly-damped out-of-plane vibrational modes can be overly excited. A second important issue in the area of 3-D motion is that of 3-D fouling, or tangling, of the wire booms during deployment. Although nominally a planar deployment, as depicted in Fig. 2, asymmetry of the initial conditions or of the spacecraft can excite 3-D response during deployment. In extreme situations this 3-D response might result in fouling of the wires.

The next three sections of this paper develop dynamic models of this system and investigate the system's behavior via analysis and simulation of these models. Section II develops two differential equation models for the system, a 3-D model, and a symmetric, planar 2-D model. Section II also develops models of the collisions that happen when the cables become fully unwrapped. Section III uses the planar model and

its linearization to analyze the system's energy dissipation and to show how to tune the system for rapid energy dissipation and robust performance. Section IV considers the 3-D motions of the system, including the stability of the final equilibrium and the nonlinear transient response during deployment.

II. Mathematical Models of the System's Dynamics

Modeling Assumptions

The three-dimensional model of this system makes a number of assumptions. The main part of the spacecraft is assumed to be a rigid body, and the ring is assumed to be a second rigid body. There is only a single rotational degree of freedom between the two bodies. No external forces or torques are considered; therefore, the system's total linear and angular momentum are both conserved. This means that the final spin rate will be lower than the initial spin rate due to the increase in the final spin-axis moment of inertia as compared to its initial value.

The wire booms are each modeled as consisting of a massless, fixed-length cable with a concentrated point mass at the tip. In effect, this model only considers the first mode of the string vibrations, as in Refs. 1 and 2. Those references modeled the booms as physical pendula, i.e., with distributed mass. In the present case, the massless-cable model is justified by the low linear densities of the cables envisioned and by the sizes of the tip masses that are needed in order to ensure stability of the 3-dimensional motion.

The cable wrapping/unwrapping model is significant. When wrapped, each cable is assumed to lie on a cylindrical helix of constant radius. The helix is assumed to be enforced by grooves in the ring. Each cable is assumed to have no bending stiffness. This fact, combined with the assumption of grooves in the ring, implies that each cable's direction may change discontinuously at the point where the unwrapped portion intersects the wrapped portion. This discontinuity must lie in the plane that is locally tangent to the ring's helix; otherwise, the cable would unwrap more and go slack. The cable is assumed to remain under tension at all times. The validity of this latter assumption during the transient part of the deployment will be checked via simulation.

Damping in the system is assumed to arise from two sources. One is the damper between the ring and the main spacecraft body. This damper is modeled with a viscous damping law that includes a term proportional to the relative angular rate and a second term proportional to the square of the relative angular rate – a later section will explain why the squared term is needed. One possible way to implement such a damper would be to use a combination of a viscous damper and a centrifugal brake. Alternatively, this damping law could be implemented actively.

The other damping source is from hysteresis in the cables when they bend. The bending is assumed to occur in a small portion of the cable near its point of attachment to the ring. Cable hysteresis is the only source of damping for some of the final equilibrium's vibration modes. This damping is modeled as being viscous and proportional to the velocity of the tip mass relative to the ring's coordinate system. This damping source is neglected when a given cable is unwrapping and enters the model only when the cable's wrap angle reaches zero.

Geometry

The geometrical model defines coordinate systems, some of the physical parameters, and the system configuration. Most of the needed geometrical quantities are depicted in Fig. 3.

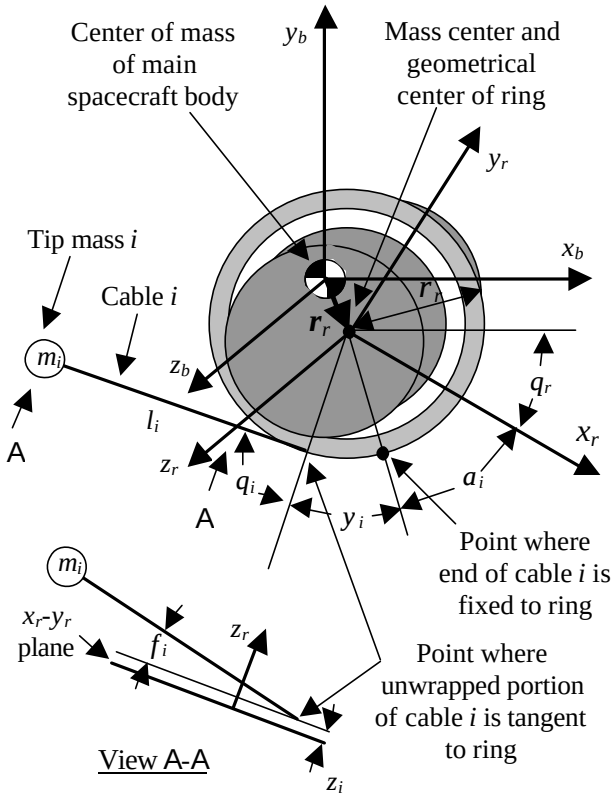

Fig. 3. Definitions of coordinate systems and geometry for the main spacecraft body, the ring, and the ith cable.

Figure 3 shows two coordinate systems and their relationship. The $[x_b, y_b, z_b]$ coordinate system is fixed to the main rigid spacecraft body. Its origin is at the center of mass of that rigid body. The $[x_r, y_r, z_r]$ coordinate system is fixed to the ring. Its origin is at the geometrical center of the ring, which is also

assumed to be the center of mass of the ring. The constant vector $\mathbf{r}_r$ gives the location of the origin of the $[x_r, y_r, z_r]$ coordinate system expressed in the $[x_b, y_b, z_b]$ coordinate system. The angle q_r gives the orientation of the $[x_r, y_r, z_r]$ coordinate system with respect to the $[x_b, y_b, z_b]$ coordinate system. It is the angle between the x_r axis and a line parallel to the x_b axis. q_r is measured positively about the $-z_r$ axis. This angle varies as the ring rotates with respect to the main spacecraft body. It is called the ring/body articulation angle. Note that the z_b and z_r axes are always parallel to each other.

The location of the ith cable and of the ith tip mass are defined in the $[x_r, y_r, z_r]$ coordinate system by 4 angles. The angle a_i is the angle between the x_r axis and the point where the base end of the ith cable is attached to the ring. This attachment point is in the x_r-y_r plane. The angle y_i is the wrap angle of the ith cable, the angle between its attachment point to the ring and the point where its unwrapped portion meets the ring. (This latter location will be called the unwrapping point throughout the remainder of the paper.) The angle q_i is the angle between the normal to the ring at the unwrapping point and the projection of the unwrapped portion of the ith cable onto the x_r-y_r plane. It is called the in-plane pendulum angle of the ith cable. Its possible values are discussed in the next paragraph. All three of these angles are measured positively about the $-z_r$ axis. The fourth angle, f_i, is depicted in view A-A in the lower left-hand corner of the figure. It is the angle between the unwrapped portion of the ith cable and its projection onto the x_r-y_r plane. It is called the out-of-plane pendulum angle.

The angles y_i and q_i are dependent. The assumption that the cable remains under tension causes q_i to take on a value of $p/2$ radians whenever the cable is unwrapping. This is so because the unwrapped portion of the cable must lie in the tangent plane of the ring at the unwrapping point. The cable is unwrapping whenever $y_i > 0$. When the cable is fully unwrapped, i.e., when $y_i = 0$, then q_i is free to take on values in the range $-p/2 \le q_i \le p/2$. Thus, at any given time, one of these two angles is constrained to a constant value.

There are two distances that help to define the ith cable's location, l_i, the length of the unwrapped portion, and z_i, the displacement of the unwrapping point above the x_r-y_r plane. This latter distance can have a negative sign in the model. These two distances are functions of the wrap angle, y_i, the total cable length, l_{if}, and the initial z_r location of the tip mass, z_{i0}:

$$l_i(y_i) = l_{if}\left[1 - \frac{r_r y_i}{\sqrt{l_{if}^2 - z_{i0}^2}}\right] \tag{1a}$$

$$z_i(y_i) = z_{i0}\left[\frac{r_r y_i}{\sqrt{l_{if}^2 - z_{i0}^2}}\right] \tag{1b}$$

where r_r is the radius of the ring's cable wrapping helix, as show in Fig. 3, and $y_i \ge 0$ is assumed. These two equations follow from the definition of a helix. It is apparent that full wrapping corresponds to $y_{i0} = [\sqrt{l_{if}^2 - z_{i0}^2}\,]/r_r$ and that the terminal value of z_i is $z_{if} = 0$.

The geometry of Fig. 3 can be used to derive two important vectors in the $[x_b, y_b, z_b]$ coordinate system. One is the position of the ith tip mass:

$$\mathbf{r}_i(q_r, y_i, q_i, f_i) = \mathbf{r}_r + \begin{bmatrix} \{r_r\cos(q_r + a_i + y_i) + l_i(y_i)\cos(f_i)\cos(q_r + a_i + y_i + q_i)\} \\ -\{r_r\sin(q_r + a_i + y_i) + l_i(y_i)\cos(f_i)\sin(q_r + a_i + y_i + q_i)\} \\ \{z_i(y_i) + l_i(y_i)\sin(f_i)\} \end{bmatrix} \tag{2}$$

The other is the unit direction vector along the ith cable pointing away from the ith tip mass:

$$\hat{\mathbf{c}}_i(q_r, y_i, q_i, f_i) = \begin{bmatrix} -\cos(f_i)\cos(q_r + a_i + y_i + q_i) \\ \cos(f_i)\sin(q_r + a_i + y_i + q_i) \\ -\sin(f_i) \end{bmatrix} \tag{3}$$

This is the direction in which the tension force of the cable acts on the tip mass.

Physical Parameters

The physical parameters of the model consist of geometrical parameters, mass properties, and damping constants. The geometrical parameters have been defined above. They are r_r, $\mathbf{r}_r$, and l_{if}, z_{i0}, and a_i for $i = 1, \ldots, N$. The model has N wire booms and tip masses.

The mass-properties parameters are m_b, I_b, m_r, I_{xxr}, I_{zzr}, and m_i for $i = 1,\ldots,N$. The mass of the main spacecraft body is m_b, and its inertia matrix about its center of mass is I_b, which is defined in the $[x_b, y_b, z_b]$ coordinate system. The mass of the ring is m_r, and its inertia matrix about its center of mass is $I_r = \mathrm{diag}[I_{xxr}, I_{xxr}, I_{zzr}]$ in the $[x_r, y_r, z_r]$ coordinate system. The ring is assumed to be axially symmetric about its center of mass/center of rotation. The value of the ith cable's tip mass is m_i. The total mass of the system is $m_{tot} = m_b + m_r + m_1 + \ldots + m_N$.

The three damping constants of the model are b_{rb1}, b_{rb2}, and b_c. The quantities b_{rb1} and b_{rb2} are the torsional damping constants between the main spacecraft body and the ring, with the coefficient b_{rb1} for the linear damping term and the coefficient b_{rb2} for the squared term. The quantity b_c is the effective linear viscous

damping at each tip mass due to its cable's bending hysteresis.

A nominal set of preliminary design parameters for the SIERRA mission will be used in much of the remainder of this paper. These nominal parameters are:

$N = 4$ cables and tip masses
$r_r = 0.127\ m$
$\mathbf{r}_r = \mathbf{0}\ m$
$l_{if} = 2.5\ m$ for $i = 1, \ldots, 4$
$z_{i0} = (-1)^{i+1}(0.015)\ m$ for $i = 1, \ldots, 4$
$a_i = (i-1)p/2\ rad$ for $i = 1, \ldots, 4$
$m_b = 29.5\ kg$
$I_b = \text{diag}[0.618, 0.618, 0.343]\ kg\text{-}m^2$
$m_r = 1.475\ kg$,
$I_{xxr} = 0.0119\ kg\text{-}m^2$
$I_{zzr} = 0.0238\ kg\text{-}m^2$
$m_i = 0.5\ kg$ for $i = 1, \ldots, 4$
$b_{rb1} = 0.1096\ N\text{-}m\text{-}sec/rad$
$b_{rb2} = 0.0084\ N\text{-}m\text{-}sec^2/rad^2$
$b_c = 0.015\ N\text{-}sec/m$

These parameters define a design that is axially symmetric about the z_b axis and symmetric with respect to the x_b-y_b plane.

Equations of Motion

The Newton-Euler formulation has been used to derive the system's equations of motion. This is a convenient method because the cable tension constraint forces need to be calculated in order to verify the no-slackness assumption and in order to model some collisions that occur.

System State Vector. The system model has $7 + 2N$ degrees of freedom. The main spacecraft body has 6 degrees of freedom, the ring articulation angle is a 7th degree of freedom, and each of the N tip masses has 2 degrees of freedom. Each tip mass undergoes translational motion that is restricted to a two-dimensional manifold. Each tip mass' manifold is defined by the fixed length of the cable, by the assumption that the cable never goes slack, and by the assumption that, when the cable is still unwrapping, the unwrapped portion of the cable remains in the plane that is tangent to the wrapping helix at the unwrapping point.

Six of the generalized coordinates and three of the generalized velocities can be eliminated from the analysis. The position coordinates of the system's center of mass and the inertial orientation coordinates of the main spacecraft body are all ignorable because they do not enter the dynamic model. The inertial velocity components of the system's center of mass do not enter the analysis because of the lack of external forces. If the inertial coordinate system is defined so that these velocities are initially zero, then they will remain zero forever.

The system state vector is defined mostly in terms of the configuration angles of Fig. 3:

$$\mathbf{x} = [\mathbf{w}_b^T,\ q_r,\ \dot{q}_r,\ y_1,\ q_1,\ f_1, \dot{y}_1,\ \dot{q}_1,\ \dot{f}_1,\ \ldots,\ y_N, q_N, f_N, \dot{y}_N,\ \dot{q}_N,\ \dot{f}_N]^T \quad (4)$$

The vector $\mathbf{w}_b$ is the inertial angular velocity of the $[x_b, y_b, z_b]$ coordinate system expressed in that system.

This state vector has $2N$ more elements than the minimum number that would be needed given the number of degrees of freedom and the number of ignorable coordinates and known velocities. The extra elements in the state vector come from the fact that y_i and q_i and their time derivatives are both retained in the state vector. As stated above, one of these angles is constrained to be a constant at any given time. The retention of both angles in the state vector is a matter of convenience that simplifies the writing of the equations of motion. This means that the dynamic model must include logic to determine which quantity is constrained at any given time. Also, it must include a model of the collision that occurs at the transition from one constraint to the other. This transition occurs when the cable first reaches its fully unwrapped state.

Kinematics. The position of the system's center of mass is an important quantity. It defines the origin of an inertial coordinate system and is needed for determining inertial velocities and accelerations. Expressed in the $[x_b, y_b, z_b]$ coordinate system, it is:

$$\mathbf{r}_{cm}(q_r, y_1, q_1, f_1, \ldots, y_N, q_N, f_N) = \frac{1}{m_{tot}}\left\{ m_r \mathbf{r}_r + \sum_{i=1}^{N} m_i \mathbf{r}_i(q_r, y_i, q_i, f_i) \right\} \quad (5)$$

Using the usual laws for deriving inertial rates of change of a vector in terms of rates of change in a non-inertial coordinate system, the inertial velocities of the centers of mass of all of the system components can be expressed in the $[x_b, y_b, z_b]$ coordinate system as follows:

$$\mathbf{v}_b = -\dot{\mathbf{r}}_{cm} - \mathbf{w}_b \times \mathbf{r}_{cm} \quad (6a)$$

$$\mathbf{v}_r = -\dot{\mathbf{r}}_{cm} + \mathbf{w}_b \times (\mathbf{r}_r - \mathbf{r}_{cm}) \quad (6b)$$

$$\mathbf{v}_i = \dot{\mathbf{r}}_i - \dot{\mathbf{r}}_{cm} + \mathbf{w}_b \times (\mathbf{r}_i - \mathbf{r}_{cm}) \quad \text{for } i = 1, \ldots, N \quad (6c)$$

where $\mathbf{v}_b$ is the inertial velocity of the main spacecraft body's center of mass, $\mathbf{v}_r$ is the inertial velocity of the ring's center of mass, and $\mathbf{v}_i$ is the inertial velocity of the ith tip mass.

In eqs. (6a)-(6c) the quantities $\dot{\mathbf{r}}_{cm}$ and $\dot{\mathbf{r}}_i$ are the time rates of change of $\mathbf{r}_{cm}$ and $\mathbf{r}_i$ with respect to the $[x_b, y_b, z_b]$ axes. Expressions for these time rates of change can be derived from eqs. (2) and (5) by using the chain rule. The resulting expressions are sums of terms,

each of which is a partial derivative with respect to an angle multiplied by that angle's rate. These expressions are straightforward to derive, and they have been omitted for the sake of brevity.

Similarly, the inertial accelerations of the components' mass centers are:

$$\boldsymbol{a}_b = -\ddot{\boldsymbol{r}}_{cm} - \dot{\boldsymbol{w}}_b \times \boldsymbol{r}_{cm} - 2\boldsymbol{w}_b \times \dot{\boldsymbol{r}}_{cm} - \boldsymbol{w}_b \times (\boldsymbol{w}_b \times \boldsymbol{r}_{cm}) \quad (7a)$$

$$\boldsymbol{a}_r = -\ddot{\boldsymbol{r}}_{cm} + \dot{\boldsymbol{w}}_b \times (\boldsymbol{r}_r - \boldsymbol{r}_{cm}) - 2\boldsymbol{w}_b \times \dot{\boldsymbol{r}}_{cm} + \boldsymbol{w}_b \times [\boldsymbol{w}_b \times (\boldsymbol{r}_r - \boldsymbol{r}_{cm})] \quad (7b)$$

$$\boldsymbol{a}_i = \ddot{\boldsymbol{r}}_i - \ddot{\boldsymbol{r}}_{cm} + \dot{\boldsymbol{w}}_b \times (\boldsymbol{r}_i - \boldsymbol{r}_{cm}) + 2\boldsymbol{w}_b \times (\dot{\boldsymbol{r}}_i - \dot{\boldsymbol{r}}_{cm}) + \boldsymbol{w}_b \times [\boldsymbol{w}_b \times (\boldsymbol{r}_i - \boldsymbol{r}_{cm})] \quad \text{for } i = 1, \ldots, N \quad (7c)$$

where $\boldsymbol{a}_b$ is the main spacecraft body's inertial acceleration, $\boldsymbol{a}_r$ is the ring's inertial acceleration, and $\boldsymbol{a}_i$ is the ith tip mass' inertial acceleration.

The quantities $\ddot{\boldsymbol{r}}_{cm}$ and $\ddot{\boldsymbol{r}}_i$ are the accelerations of $\boldsymbol{r}_{cm}$ and $\boldsymbol{r}_i$ with respect to the $[x_b, y_b, z_b]$ coordinate system. Derivable via the chain rule from the expressions for $\dot{\boldsymbol{r}}_{cm}$ and $\dot{\boldsymbol{r}}_i$, their expressions consist of sums of two types of terms. One type of term is a partial derivative of the corresponding $\boldsymbol{r}$ vector with respect to an angle multiplied by the second time derivative of that angle, e.g., $[\partial \boldsymbol{r}_{cm}/\partial q_r]\ddot{q}_r$. The other type of term is a second partial derivative of the $\boldsymbol{r}$ vector with respect to two angles multiplied by the first time derivatives of those two angles, e.g., $[\partial^2 \boldsymbol{r}_i/(\partial q_r \partial f_i)]\dot{q}_r \dot{f}_i$. The full expressions for $\ddot{\boldsymbol{r}}_{cm}$ and $\ddot{\boldsymbol{r}}_i$ are straightforward to derive and are omitted for the sake of brevity.

Interaction Forces and Torques. There are various forces and torques that act between the different bodies of this system. Most of these enforce constraints, but two arise from damping constitutive laws.

The main spacecraft body interacts with the ring via a force vector and a moment vector. The force vector is a constraint force that keeps the ring at the constant position $\boldsymbol{r}_r$ in the spacecraft body's coordinate system. Call this force $\boldsymbol{f}_{rb}$. It acts positively on the ring and negatively on the spacecraft body, and it is applied to both bodies at the position $\boldsymbol{r}_r$. The moment vector consists of *2* constraint torque components and one damping torque component: $\boldsymbol{n}_{rb} = [n_{rb1}, n_{rb2}, (b_{rb1}\dot{q}_r + b_{rb2}\dot{q}_r|\dot{q}_r|)]^T$. This moment vector acts positively on the ring and negatively on the spacecraft body. The constraint torques and forces, n_{rb1}, n_{rb2}, and the three elements of $\boldsymbol{f}_{rb}$, are unknowns that will be determined from the dynamic equations.

Each tip mass interacts with the ring through its cable's tension force and hysteresis damping force. The total force that acts on each tip mass is

$$\boldsymbol{f}_i = T_i \hat{\boldsymbol{c}}_i(q_r, y_i, q_i, f_i) - \begin{cases} 0 & \text{if } y_i > 0 \\ b_c\left(\dot{q}_i \dfrac{\partial \boldsymbol{r}_i}{\partial q_i} + \dot{f}_i \dfrac{\partial \boldsymbol{r}_i}{\partial f_i}\right) & \text{if } y_i = 0 \end{cases} \quad \text{for } i = 1, \ldots, N \quad (8)$$

where T_i is the tension in the ith cable. The second term, which models the hysteresis damping, is nonzero only when the cable is fully unwrapped. The term in parentheses in the lower line of the second term is the ring-relative velocity of the ith tip mass expressed in $[x_b, y_b, z_b]$ coordinates. The force $\boldsymbol{f}_i$ is also expressed in $[x_b, y_b, z_b]$ coordinates. It acts at the ith tip mass. The corresponding force on the ring is $-\boldsymbol{f}_i$. The unknown tension constraint forces, T_i for $i = 1, \ldots, N$, will be determined from the dynamic equations.

Equations of Motion and Computation of State Rates. The Newton-Euler equations of motion for the system are:

$$m_b \boldsymbol{a}_b = -\boldsymbol{f}_{rb} \quad (9a)$$

$$I_b \dot{\boldsymbol{w}}_b + \boldsymbol{w}_b \times \{I_b \boldsymbol{w}_b\} = -\boldsymbol{n}_{rb} - \boldsymbol{r}_r \times \boldsymbol{f}_{rb} \quad (9b)$$

$$m_r \boldsymbol{a}_r = \boldsymbol{f}_{rb} - \sum_{i=1}^{N} \boldsymbol{f}_i \quad (9c)$$

$$I_r\left(\dot{\boldsymbol{w}}_b + \begin{bmatrix} 0 \\ 0 \\ -\ddot{q}_r \end{bmatrix}\right) + \boldsymbol{w}_b \times \left\{I_r\left(\boldsymbol{w}_b + \begin{bmatrix} 0 \\ 0 \\ -\dot{q}_r \end{bmatrix}\right)\right\} = \boldsymbol{n}_{rb} - \sum_{i=1}^{N} (\boldsymbol{r}_i - \boldsymbol{r}_r) \times \boldsymbol{f}_i \quad (9d)$$

$$m_i \boldsymbol{a}_i = \boldsymbol{f}_i \quad \text{for } i = 1, \ldots, N \quad (9e)$$

Equations (9a)-(9e) constitute a set of $12 + 3N$ equations in $9 + 3N$ unknowns. Even though this system of equations is over determined, it is solvable because it is compatible. Equations (9a), (9c), and (9e) for $i = 1, \ldots, N$ are linearly dependent; they add up to yield $\boldsymbol{0} = \boldsymbol{0}$. Linear dependence holds because the net external force is zero and because this fact has been used to derive the expressions for the inertial accelerations in eqs. (7a)-(7c). Equation (9c) can be eliminated without loss of information, which leaves a system of $9 + 3N$ equations in $9 + 3N$ unknowns.

The unknowns in these equation can be determined by a matrix inversion. Given that the values of the states defined in eq. (4) are known, the unknowns in eqs. (9a), (9b), (9d), and (9e) are the generalized constraint forces, $\boldsymbol{f}_{rb}$, n_{rb1}, n_{rb2}, and T_i for $i = 1, \ldots, N$, and the generalized coordinate accelerations, $\dot{\boldsymbol{w}}_b$, $\ddot{q}_r$, $(\ddot{y}_1 \text{ or } \ddot{q}_1)$, $\ddot{f}_1, \ldots, (\ddot{y}_N \text{ or } \ddot{q}_N)$, and $\ddot{f}_N$. The only

generalized accelerations that enter eqs. (9a), (9b), (9d), and (9e) explicitly are $\dot{\boldsymbol{w}}_b$ and $\ddot{q}_r$. The other generalized accelerations enter through the expressions for $\ddot{\boldsymbol{r}}_{cm}$ and $\ddot{\boldsymbol{r}}_i$, which are components of $\boldsymbol{a}_b$, $\boldsymbol{a}_r$, and $\boldsymbol{a}_i$, respectively. Each of the unknowns enters the equations linearly. Therefore, the equations can be solved by a matrix inversion. The resulting system of equations is nonsingular if all of the lengths of the unwrapped portions of the cables, l_i for $i = 1, \ldots, N$, are nonzero. This is the case for all situations considered in this paper. Where needed in the ensuing analysis or simulations, the required matrix inversion has been carried out numerically.

The state rate vector $\dot{\boldsymbol{x}}$ is computable once the dynamics equations have been solved for their unknowns. The rates of change of the generalized coordinates in the $\boldsymbol{x}$ vector are readily available as the generalized velocities in that same vector. The generalized accelerations are available either from the solution of the dynamics equations are from constraints. While the ith cable is unwrapping, $\ddot{y}_i$ is available from the dynamics equations, and $\ddot{q}_i$ is set equal to zero. After the completion of the unwrapping process, after y_i hits zero, the situation reverses: $\ddot{q}_i$ is available from the dynamics equations, and $\ddot{y}_i$ is set equal to zero.

Collision when a Cable Reaches the State of Being Fully Unwrapped

A collision occurs if $z_{i0} \neq l_{if}\, sin(f_i)$ at the moment that y_i hits zero. The angular rate $\dot{y}_i$ changes abruptly from a negative value to 0, and $\dot{q}_i$ changes abruptly from 0 to a negative value. The velocity $\dot{\boldsymbol{r}}_i$ is discontinuous because $\partial \boldsymbol{r}_i / \partial y_i$ and $\partial \boldsymbol{r}_i / \partial q_i$ are not linearly dependent.

It is straightforward to calculate what happens in the collisions. The basic assumption of the collision is that the cable remains taut after the collision. All of the nonzero generalized velocities can undergo discontinuous changes during one of these collisions, and all of the generalized constraint forces can experience impulses. The way to solve for these velocity changes and impulses is to enforce conservation of total system angular momentum while enforcing the required change in $\dot{y}_i$ from a pre-collision negative value to zero.

The collision model uses the same dynamics matrix that multiplies the vector of unknown generalized constraint forces and generalized accelerations in the dynamics equations. This matrix is set to its post-collision configuration, i.e., with a column for $\ddot{q}_i$ but no column for $\ddot{y}_i$. The column that gets dropped, the column for $\ddot{y}_i$, is then left-multiplied by the inverse of the new dynamics matrix, and the result is multiplied by the value of $\dot{y}_i$ just prior to the collision. The resulting solution vector contains the step changes to the generalized velocities and the impulses that occur in the generalized forces.

Typically, the cable tension impulses are negative for all of the cables other than the cable that is directly involved in the collision. Despite appearances, this does not seriously violate the modeling assumption that all cables are always taut. The negative impulse levels are so low in comparison to the nominal tensions that the cables' slack times are negligibly small, on the order of milliseconds or less.

Symmetric, Planar Equations of Motion

If the system is symmetrical and if it starts out with planar and symmetrical initial conditions, then its motion stays planar and symmetrical, and it can be analyzed with a low-dimensional model. This model captures the basic energy dissipation mechanism in this system.

The following assumptions assure planar symmetrical motions: The main spacecraft body axes $[x_b, y_b, z_b]$ are principal axes: $I_b = \text{diag}[I_{xxb}, I_{yyb}, I_{zzb}]$. The ring's center and the main spacecraft body's center of mass coincide: $\boldsymbol{r}_r = \boldsymbol{0}$. The initial spin vector is directed along the z_b axis: $\boldsymbol{w}_b(t_0) = [0,0,w_{z0}]^T$. All of the tip masses and cable lengths are the same: $m_i = m_{tip}$ and $l_{if} = l_f$ for $i = 1, \ldots, N$. The N cables' attachment points to the ring are equally distributed around the circumference of the ring: $(a_{i+1} - a_i) = 2p/N$. All of the initial tip-mass out-of-plane displacements and velocities are zero, and the cable wrapping helix has negligible out-of-plane height: $f_i(t_0) = 0$, $\dot{f}_i(t_0) = 0$, and $z_{i0} = 0$. All of the initial tip-mass in-plane displacements and velocities are the same: $y_i(t_0) = y(t_0)$, $\dot{y}_i(t_0) = \dot{y}(t_0)$, $q_i(t_0) = q(t_0)$, and $\dot{q}_i(t_0) = \dot{q}(t_0)$ for $i = 1, \ldots, N$. For convenience' sake, this model also assumes that the cable hysteresis damping is zero: $b_c = 0$.

The symmetric, planar equations of motion are:

$$I_{zzb}\, \dot{w}_z = -b_{rb1}\, \dot{q}_r - b_{rb2}\, \dot{q}_r |\dot{q}_r| \tag{10a}$$

$$I_{zzr}\, (\dot{w}_z - \ddot{q}_r) = b_{rb1}\, \dot{q}_r + b_{rb2}\, \dot{q}_r |\dot{q}_r| - N r_r T \sin(q) \tag{10b}$$

$$m_{tip} \{ l(\dot{w}_z - \ddot{q}_r - \ddot{q} - \ddot{y}) + r_r(\dot{w}_z - \ddot{q}_r)\cos(q) - r_r(w_z - \dot{q}_r - \dot{y})^2 \sin(q) - 2\, r_r \dot{y}\, (w_z - \dot{q}_r - \dot{y}) - r_r \ddot{y} \cos(q) + r_r \dot{y} \dot{q} \} = 0 \tag{10c}$$

$$T = m_{tip}\{l(w_z - \dot{q}_r - \dot{q} - \dot{y})^2 + r_r(\dot{w}_z - \ddot{q}_r)sin(q) + r_r(w_z - \dot{q}_r - \dot{y})^2 cos(q) + r_r\ddot{y}[1 - sin(q)]\} \quad (10d)$$

where T is the tension of each cable, and $l = l_f - r_r y$ is the length of the unwrapped portion of each cable. Note, the angles q and y do not have subscripts in these equations because these angles remain the same for each of the N cables.

As with the 3-dimensional model, this model has two phases of operation, an unwrapping phase and a totally unwrapped phase. The constraints for the unwrapping phase are $y > 0$ and $q = p/2$. The constraints for the totally unwrapped phase are $y = 0$ and $-p/2 \le q \le p/2$. The transition between the two phases occurs when y just reaches a value of zero. At this point it will have a negative rate, $\dot{y} < 0$. At the transition $\dot{y}$ jumps instantaneously to zero, and $\dot{q}$ jumps from zero to the pre-transition negative value of $\dot{y}$. This model of the transition conserves both angular momentum and energy.

III. Performance of the Energy Dissipation System

Simulation of a Nominal Case

The performance of the energy dissipation device can be evaluated by nonlinear simulation of the symmetric planar equations of motion, eqs. (10a)-10d). Simulation is the most expedient tool because the equations are nonlinear.

The nominal case has been run using the parameters of the preliminary design for the SIERRA mission, which are given above. The initial spin rate was chosen to be $w_z = 25.642$ *rad/sec.* Some representative time histories for this case are plotted in Fig. 4.

The top plot of Fig. 4 shows the total energy as it decays with time. The final system moment of inertia is *35.5* times larger than the initial moment of inertia; so, the final energy is *35.5* times smaller than the initial energy. This plot shows that almost all of the excess energy gets dissipated in the first *5* seconds of deployment. The middle plot shows the cable wrapping angle time history, $y(t)$, and the time history of the articulation angle between the ring and the main spacecraft body, $q_r(t)$. The units on this plot are revolutions. $y(t)$ starts at a value of l_f / r_r radians, which is *3.13* revolutions, and it unwinds to zero in under *5* seconds. The articulation angle starts at zero and decreases to *–6* revolutions by the time the deployment is complete. The lower plot shows the in-plane cable pendulum angle time history, $q(t)$, in degrees. It starts out at $+90^o$ and stays at that value all during the unwrapping phase, consistent with previously stated assumptions. The pendulum angle quickly decays to zero after the cables have fully unwrapped, but with some undershoot. The undershoot does not reach -90^o; so, the cables do not begin to re-wrap around the ring.

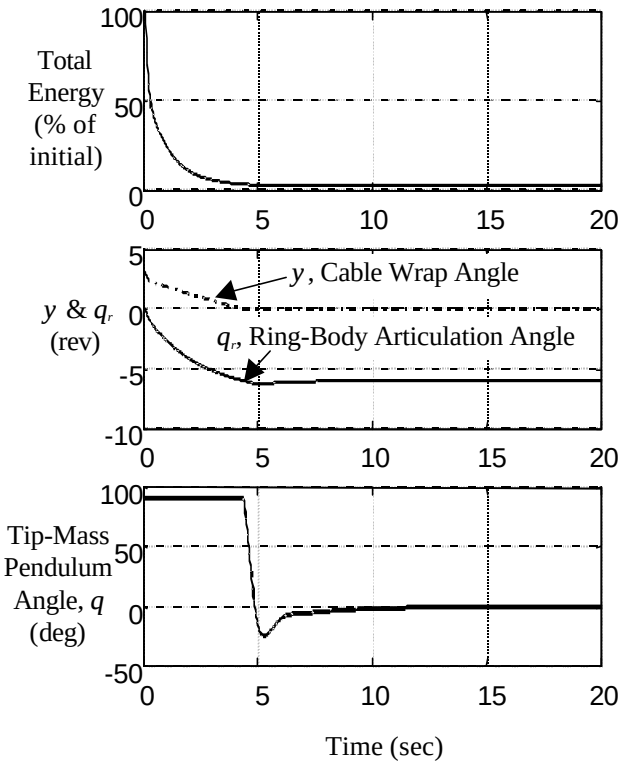

Fig. 4. Transient deployment time histories for the planar, symmetrical model and the nominal design parameters.

These plots show excellent performance of the system. The pendulum angle, $q(t)$, is less than a degree after *12* seconds, and the energy is less than *0.02*% above its final equilibrium value. These results indicate that the proposed system can be used on a sounding rocket flight.

The one drawback of the system is the large final articulation angle, $q_r(t)$. The system will need to get electrical signals from the main spacecraft body to the cable's tip masses and back. In order to do this, it will need to use some sort of wire spooling system or wire wrap that allows a hard-wired connection to be maintained over the large articulation angle range. Also, the system will need to know the value of $q_r(t)$ in order to estimate where the tip masses are in spacecraft coordinates. Therefore, an angle sensor will be needed as part of the system.

Performance Robustness in the Presence of Modeling Uncertainty

The deployment system's performance must not degrade too rapidly as the parameters vary from their nominal values. An actual flight system will exhibit differences from the model that has been used to design the deployment system. If the system's performance is not robust with respect to the expected levels of such differences, then an actual system may not deploy properly.

Robustness has been tested by simulating deployments with sets of model parameters that vary from those given above for the nominal design. Each deployment corresponds to a set of parameters that have been (pseudo) randomly chosen from a flat probability distribution which is centered at the nominal value. The ranges of the variations for the parameters m_{tip}, I_{zzb}, I_{zzr}, r_r, and l_f all have been set at ± *5*% of their nominal values. The parameters b_{rb1} and b_{rb2} and the initial spin rate $w_z(t_0)$ have been allowed to vary ± *25*% from their nominal values. These parameter variation ranges have been chosen conservatively and are based on manufacturing tolerances, typical measurement accuracies, and variations of flight initial conditions that have been experienced by some of the authors.

All of the off-nominal deployments that have been simulated show acceptable performance. Figure 5 presents two deployment angle time histories for a set of *15* cases with parameter variations as described. None of them show any possibility of the cables tending to re-wrap. Re-wrapping in the direction of the original wrapping would be indicated by a zero or negative unwrap rate – a zero or negative slope of the top plot – before y reaches zero. Re-wrapping in the direction opposite to the original wrapping would be indicated by a pendulum angle that violated the lower bound of the range $-90^o \le q \le 90^o$. All of the settling times are very fast: the pendulum angle stays less than 1^o after *16.25* sec in all *15* cases.

Two different situations cause conditions that would lead to temporary cable re-wrapping and possible fouling if they were exacerbated by increases in the parameter variations. One such situation is the case that yielded a q undershoot of -66^o on Fig. 5. This case started with the following problematic combination of parameter variations: the lowest possible initial spin rate, $w_z(t_0)$, and the highest possible damping parameters, b_{rb1} and b_{rb2}. In the situation of a very low spin rate or of very high damping, the system tends to act more like the original yo-yo system. Not enough energy dissipation occurs by the time the cables unwrap, and the pendulum angle exhibits undershoot that can lead to re-wrapping in extreme situations.

The other situation of concern is that of the cable re-wrapping in its original direction of wrap. If larger parameter variations are allowed, then this can happen early on in the deployment process, before the cables are fully unwrapped. As can be seen on the top plot of Fig. 5, the initial unwrap rate, the slope of the curve, is large in magnitude and negative. In less than *0.5* sec. the unwrapping rate slows down to an almost constant rate that it maintains for the remainder of the unwrapping phase. Depending on the values of the uncertain parameters, the unwrapping rate can become temporarily negative during the early speed transition. In this situation the cables temporarily re-wrap, which could lead to fouling. The parameter variations that tend to cause temporary re-wrapping are those of low rotary damping, i.e., of b_{rb1} and b_{rb2} values that are lower than their nominals. In particular, too low of a square-law damping constant, b_{rb2}, tends to lead to cable re-wrapping during this initial phase.

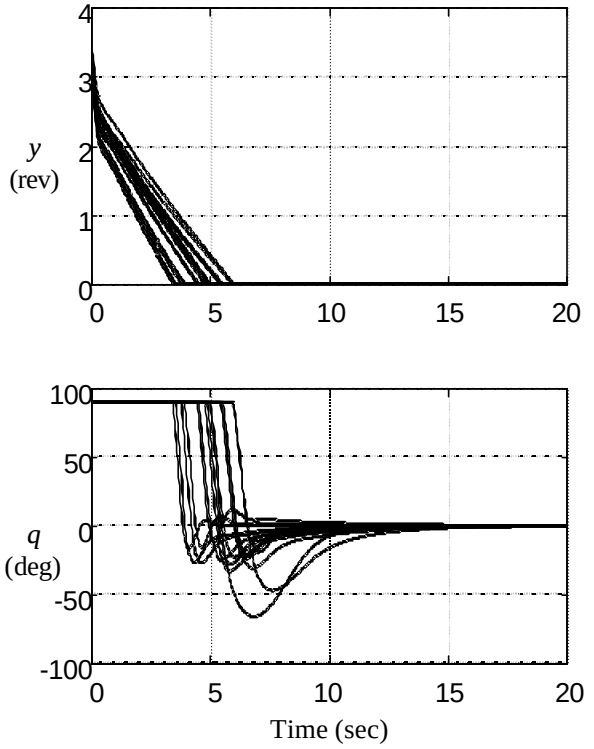

Fig. 5. Unwrap-angle and in-plane pendulum-angle deployment time histories for a set of planar, symmetrical cases with varying design parameters.

Tuning of the Damping Constants

It is necessary to tune the damping constants b_{rb1} and b_{rb2} in order to achieve rapid deployment while avoiding possible re-wrapping that could lead to fouling of cables. If the damping values are too low,

then the system will require too much time to dissipate enough energy in order to complete its deployment. Also, if b_{rb2} is too low, then cable re-wrapping can occur during the initial unwrapping phase. If the damping values are too high, on the other hand, then not enough energy will be dissipated by the time the cables are fully unwrapped because not enough ring-body articulation motion will have been allowed to occur. Large undershoot of q will occur, which will lead to re-wrapping in the opposite direction from the original wrapping.

Good tuning of b_{rb1} can be achieved by considering the characteristic values of the linearization of the planar, symmetrical system about its steady-state deployed configuration, $\dot{q}_r = \dot{q} = \dot{y} = 0$ and $q = y = 0$. The system has a five-dimensional state vector in this case, $\boldsymbol{x} = [w_z,\ q_r,\ \dot{q}_r,\ q,\ \dot{q}\ ]^T$. Two of the five characteristic values of the system are identically zero. These correspond to the q_r and w_z modes, which are neutrally stable for obvious reasons. The other 3 characteristic values vary as a function of b_{rb1}. This variation is depicted in the root locus of Fig. 6.

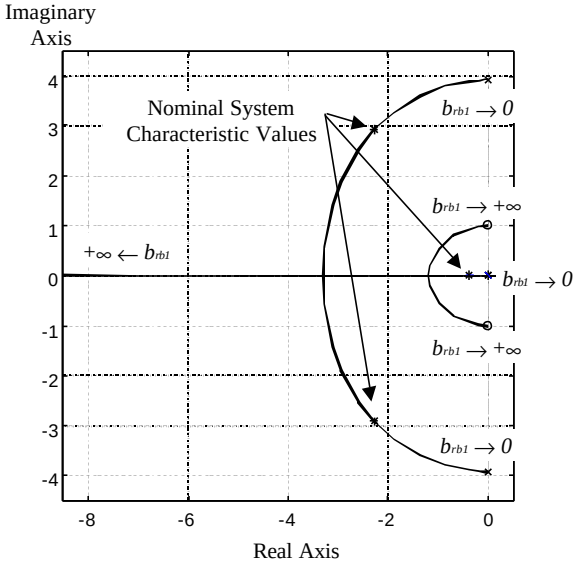

Fig. 6. The b_{rb1} (viscous damping constant) root locus for the linearization of the planar, symmetrical system.

Good tuning of b_{rb1} places the system characteristic values sufficiently far to the left of the imaginary axis to attain a reasonable settling time, but not so far to the left as to cause b_{rb1} to be too large, which would cause too much undershoot of q. A reasonable trade-off between speed and avoiding too much undershoot is found when the characteristic value on the branch that starts at $s = 0$ is about *1/4* to *1/2* of the way to the root locus' first break-away point. For the nominal system roots depicted on Fig. 6, this corresponds to a system characteristic value of $s = -0.368$, which yields a linearized-system *2%* settling time of *4/0.368 = 10.9* sec. This is about the same as the nonlinear deployment settling time that was determined via simulation. If b_{rb1} is much larger, then the characteristic values tend to split and head towards their $b_{rb1} = +\infty$ values at $s = \pm j$. At these values the system re-wraps due to excessive q undershoot. Even at lesser nominal values of b_{rb1}, the system can re-wrap if the actual spacecraft has more damping than expected and a lower-than-expected initial spin rate.

The requirement that $\dot{y}$ remain negative during the unwrapping phase provides a criterion for tuning b_{rb2}. Figure 7 presents four different plots of $\dot{y}(t)$ for four different values of b_{rb2}, the nominal value, and values that are a half, a quarter, and an eighth of this value. As can be seen from the figure, the peak value of $\dot{y}(t)$ increases as b_{rb2} decreases, and vice versa. Thus, from the standpoint of avoiding a positive $\dot{y}$, it is good to use a large b_{rb2}. Another benefit of using a larger b_{rb2} is that the total change in the ring-body articulation angle, q_r, gets lowered as b_{rb2} increases If b_{rb2} is too large, however, q undershoot problems can occur at a later stage of the deployment. A good tradeoff seems to occur when b_{rb2} is just large enough to essentially eliminate all of the overshoot after the rapid decay of $\dot{y}(t)$ from its large initial negative value. As can be seen from Fig. 7, this is just the value of b_{rb2} that has been chosen as the nominal.

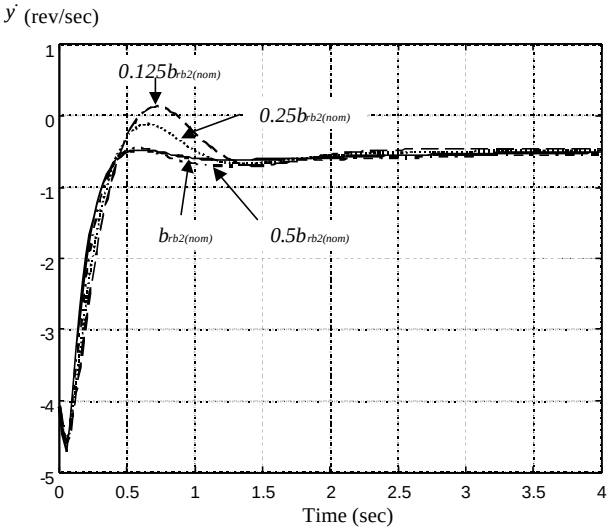

Fig. 7. Cable unwrapping rate time histories for four different values of the squared-law damping coefficient, b_{rb2}.

IV. Three-Dimensional Motion of the System

Two aspects of the system's three-dimensional motion must be considered. One important aspect is the stability of the final configuration. If it is not sufficiently stable, then the system may enter another steady state or it may take too long to settle down to its steady state after experiencing three-dimensional perturbations. Another important aspect is the transient response. Various asymmetries can arise in the system. These include those due to manufacturing tolerances and those due to asymmetric initial conditions. These will excite three-dimensional transient motions during the deployment. If the magnitudes of these motions are too large, then cables may foul on the spacecraft or on each other.

Three-Dimensional Stability of the Final Equilibrium

The three-dimensional stability of the symmetrical four-tip-mass system will be considered. This system's final desired equilibrium is defined by $\dot{q}_r = 0$, $\dot{q}_i = \dot{y}_i = \dot{f}_i = 0$ for $i = 1,\ldots, 4$, and $q_i = y_i = f_i = 0$ for $i = 1,\ldots, 4$. The linearized system state vector at this equilibrium has *21* elements:

$$\boldsymbol{x} = [\boldsymbol{w}_b^T, q_r, \dot{q}_r, q_1, f_1, \dot{q}_1, \dot{f}_1, \ldots, q_4, f_4, \dot{q}_4, \dot{f}_4]^T \quad (11)$$

This system's 21×21 linearized dynamic equations have *9* oscillatory modes and *3* real modes. Eight of the oscillatory modes are associated with vibrations of the 4 cables, 4 being in-plane modes and 4 being out-of-plane modes. The shapes of these modes are roughly those depicted in Fig. 4 of Ref. 1. The ninth oscillatory mode is the nutation model, but with modifications due to the effects of the wire booms.

Two of the three real modes have a characteristic value of zero. These are the system spin mode and the ring-body articulation mode. The zero characteristic value of the spin mode is a result of the conservation of angular momentum. The articulation mode's characteristic value is zero because there is no torsional stiffness in the connection between the main spacecraft body and the ring.

The third real mode is the articulation angle rate mode, the $\dot{q}_r$ mode. This mode normally has a rapid decay time constant due to the damping in the ring-body connection, b_{rb1}, and due to the damping in the cable hysteresis, b_c.

There is a very important stability criterion for the nutation mode of the system. In normal passive, torque-free rigid-body motion, the global stability criterion for the nutation mode is that the spin occur about the principal axis with the maximum moment of inertia. This condition ensures global stability because the equilibrium will have the minimum energy for a given angular momentum. In a torque-free environment, angular momentum is always conserved, even if rigidity assumptions are slightly violated, but violation of the rigidity assumptions usually creates the possibility for energy loss. Therefore, the spacecraft will tend to its minimum-energy spin state for a given magnitude of the angular momentum.

There is a similar minimum-energy condition for the system in question. This condition assumes that the system is symmetric, i.e., that $\boldsymbol{r}_r = \boldsymbol{0}$, $l_{if} = l_f$ for $i = 1,\ldots,4$, $a_i = (i-1)p/2$ for $i = 1,\ldots,4$, $I_b = \text{diag}[I_{xxb};I_{xxb};I_{zzb}]$, and $m_i = m_{tip}$ for $i = 1,\ldots,4$. Given these assumptions, the following condition ensures that the desired equilibrium is the global minimum-energy state of the system for a given angular momentum:

$$I_{zzb} + I_{zzr} + 2\, m_{tip}\,(r_r^2 + r_r l_f) > I_{xxb} + I_{xxr} \quad (12)$$

This global minimum energy criterion has been derived by considering the possible equilibrium positions of each cable and of the system center of mass, all as functions of the spin vector's direction. All possible spin-vector directions and equilibrium cable locations have been analyzed in terms of their resultant effective moment of inertia about the spin axis. This analysis shows that the desired equilibrium has a higher effective spin-axis moment of inertia than all other possible equilibria if condition (12) is satisfied. The analysis does not guarantee that no other equilibrium spin condition can be a local minimum energy condition – as would surely be the case if cable fouling occurred. The analysis is long and complicated and has been omitted for the sake of brevity.

The minimum-energy condition in eq. (12) allows the system designer some flexibility in designing the main spacecraft body. It is more restrictive than if the cables were rigid cantilevered rods; the left-hand side of eq. (12) would include the term $+2m_{tip}l_f^2$ in that case. On the other hand, eq. (12) is less restrictive than if there were no wire booms; the system would be a rigid-body in this case and would have to obey the stability criterion $I_{zzb} + I_{zzr} > I_{xxb} + I_{xxr}$.

Equation (12) allows the main spacecraft body and the ring to be designed with $I_{zzb} + I_{zzr} < I_{xxb} + I_{xxr}$. For a given payload mass, such a design fits more easily inside the fairing of a sounding rocket. One can then recover stability by increasing m_{tip} until eq. (12) is satisfied as a strict inequality. If $l_f > r_r$ holds, then this is more efficient than adding mass at the perimeter of the main spacecraft body in order to modify its inertias to satisfy $I_{zzb} + I_{zzr} > I_{xxb} + I_{xxr}$. In this latter scenario the

stabilizing mass presumably would be added at or near the radius r_r.

The nominal preliminary design parameters for the SIERRA mission yield a stable final equilibrium. The desired equilibrium is the minimum-energy configuration for the system because the expression on the right-hand side of inequality (12) is only *90%* of the expression on the left-hand side. If one assumes a final spin rate of *0.737 rad/sec*, then the *21* characteristic values of the system's linearization about its equilibrium are *0, 0, -0.0133 ± 0.0503j, -0.0138 ± 0.1868j, -0.0150 ± 0.1619j, -0.0150 ± 0.7394j, -0.0160 ± 0.7629j, -0.0171 ± 0.2319j, -0.0218 ± 0.7394j, -0.3235 ± 1.0916j, -0.4980 ±0.3042j*, and *-24.6489*, all in units of *1/sec* or *rad/sec.* Except for the two modes that must have zero eigenvalues, the least negative real part of a characteristic value is *-0.0133/sec.* Although this gives a rather long time constant of *75* seconds, simulation results show that this and other slow modes of oscillation are not excited very much by the expected levels of asymmetry in the spacecraft and in the system's initial conditions before deployment.

Three-Dimensional Simulation of Deployment Transient Response

Three-dimensional simulations of eqs. (9a)-(9e) have been run in order to study the transient response of the system. Symmetrical and asymmetrical cases have been run.

If all of the design parameters and initial conditions are symmetrical, then the 3-dimensional simulations reveal little new information beyond that revealed by the simulations of the planar, symmetric model in eqs. (10a)-(10d). The only new information in such simulations has to do with the added damping due to cable hysteresis, b_c, and the level of the f_i oscillations that get excited by the nonzero values of the wire-wrap helicity parameters, z_{i0}. Neither piece of information is remarkable except to note that significant levels of damping due to cable hysteresis will decrease the amount of q_i undershoot that occurs after the wires are fully unwrapped. This decreases the likelihood of the wires re-wrapping in the opposite direction.

The nonsymmetrical transient response must be studied for one important reason: to see whether the likely levels of system and initial-condition asymmetries could cause any of the cables to contact each other or other parts of the spacecraft during the transient phase of the deployment. If this were to happen, then a wire might become fouled and fail to fully deploy. This possibility is particularly important to investigate for designs like the nominal preliminary SIERRA design because it initially spins around its minimum inertia axis; i.e., the spin-axis inertia is only *62%* of the transverse-axis inertia when the wires are stowed.

Several asymmetrical 3-dimensional simulations have been run in order to evaluate the possibility of the cables fouling. Fouling conditions did not occur in any of these cases. None of the wires approached anywhere near each other. The fouling condition that came the closest to being violated in any of the simulations was a limit on the magnitude of the f_i excursions. The maximum f_i excursion that was observed in any simulation was 73.8^o. This was a case whose damping parameters were not optimized, and it had significant levels of system and initial-condition asymmetry. When the same levels of asymmetry were simulated with well-tuned damping parameters, the maximum f_i excursion was reduced to 37.4^o.

To conclude this presentation, a result for a particular asymmetric case is presented. The case considered is the one that produced a maximum f_i excursion of 37.4^o. The primary asymmetries were in the spacecraft inertias and in the initial spin vector direction. The main spacecraft body had cross products of inertia so that the principal axis of the stowed configuration was 5.7^o away from the ring's rotational articulation axis, and the initial orientation of the spin vector was 5^o away from the ring's rotation axis and in a different direction from the error in the initial principal axis so that it started out 7.6^o away from that axis. Additional small asymmetries were introduced by the following random system irregularities: l_{if} errors in the range *±1.3 cm*, z_{i0} errors in the range *±0.13 cm*, a_i errors in the range $\pm 1.7^o$, m_i errors in the range *0* to *36 gr*, and a nonzero $\mathbf{r}_r$ = [*0.35*, *-0.7*, *1.7*] *cm.*

Figure 1 shows two snapshots of the system for this case. They correspond to the time instant when the maximum f_i excursion occurred, *9.35* sec into the deployment. It is plain from this figure that the system does not come anywhere near a situation that could cause the wire booms to get entangled with one another or to foul on part of the main spacecraft body.

V. Conclusions

A new type of wire boom deployment system has been developed for use with a spin-stabilized spacecraft. Instead of deploying the wire booms from spools, as in the traditional approach, it deploys them using a mechanism similar to a yo-yo despin device. This allows for very rapid deployment, which is needed for use with a sounding rocket mission. A ring is added to the system in order to facilitate the removal of excess system energy so that the wire booms and the yo-yo tip masses can be retained without the wires

re-wrapping about the spacecraft. The ring is free to rotate with respect to the spacecraft about the nominal spin axis, and the wire booms are initially wrapped around the ring. A nonlinear damping connection between the ring and the spacecraft provides the principal means of energy removal for the system.

The system has been analyzed and simulated using a two-dimensional symmetrical model and a three-dimensional asymmetrical model. The results of the simulations show excellent performance. A nominal design can deploy four *2.5 m* wire booms in under *12* sec. Even with a *25%* initial error in the spin rate and *25%* errors in the damping factors, the system still deploys in under *17* sec without fouling of the cables. The final equilibrium has been shown to be stable with respect to three-dimensional motion. Initial asymmetries of 5^{o} in the spin direction and in the spacecraft principal axis direction did not cause enough out-of-plane motion to present any serious risk that the wire booms would become entangled during the deployment.

Acknowledgments

This work was supported in part by NASA grant number NAG5-6987, Nano-Electric Field Technology. Andy Ruina explained why the tension constraint forces can dissipate energy.

References

1. Longman, R.W. and Fedor, J.V., "Dynamics of Flexible Spinning Satellites with Radial Wire Antennas," *Acta Astronautica*, Vol. 3, Nos. 1-2, Jan.-Feb. 1976, pp. 17-37.
2. Hubert, C., "The Attitude Dynamics of Dynamics Explorer A," AIAA Paper No. 81-123, AAS/AIAA Astrodynamics Specialist Conf., Lake Tahoe, NV, Aug. 3-5, 1981.
3. Thomson, W.T., *Introduction to Space Dynamics*, J. Wiley & Sons, (New York, 1961), pp. 208-212.
4. Kaplan, M.H., *Modern Spacecraft Dynamics and Control*, J. Wiley & Sons, (New York, 1976), pp. 188-192.
5. Wiesel, W.E., *Spaceflight Dynamics*, McGraw-Hill, (New York, 1989), pp. 141-145.
6. Schiring. E.E., Heffel, J.W., and Litz, C.J., "Simulation Modeling and Test of a Satellite Despin System," AIAA Paper No. 89-3267, AIAA Flight Simulation Technologies Conf., Boston, MA, Aug. 14-16, 1989.